Journal of
Ceramic Science
and Technology

J. Ceram. Sci. Technol., **12** [1] 49-58 (2021)
DOI: 10.4416/JCST2020-00015
available online at: http://www.ceramic-science.com

Review

Thermal Shock Resistance of ZrB_2-$MoSi_2$-SiC High-Temperature Ceramics Prepared by Spark Plasma Sintering

Y. Zhang[1, 2], J. Li*[1], W. Liu[1, 2], L. Zhang[1, 2], P. Zhu[1, 2], X. Yi[1, 2], S. Wei[2], G. Zhang[1], L. Jie[2], K. Pan[2], J. Shen[3]

[1]Material Science & Engineering School, Henan University of Science & Technology, Luoyang 471023, China
[2]Henan Key Laboratory of High-Temperature Structure and Functional Materials, Luoyang 471003, China
[3]Department of Computer & Information Science, Michigan University, Dearborn, Dearborn, 48128, US

received May 3, 2020; received in revised form November 24, 2020; accepted November 29, 2020

Abstract

In this study, ZrB_2-$MoSi_2$-based ceramics, namelyZrB_2-15$MoSi_2$, were produced by means ofspark plasma sintering technology. The effect of the amount of SiC additive on the microstructure of the oxide phase, morphology of the oxidized surface, thermophysical parameters, and thermal shock resistance were investigated with a variety of techniques, such as X-ray diffraction (XRD), scanning electron microscopy (SEM) with energy dispersive analysis (EDS), nanoindentation, and thermal expansion coefficient and laser thermal conductivity determinations. The measured thermophysical parameters indicate that SiC improves relative density and thermal conductivity, decreases the thermal expansion coefficient and elastic modulus, which is beneficial for thermal shock resistance. The investigation of the surface microstructure and cross-section of the sample after the thermal shock experiment indicates that although defects like gas pores and microcracks may be generated after the first thermal shock test, the material can self-repair with sufficient and melt-flowing SiO_2 phase in the subsequent thermal shock tests. The oxide layer consists of SiO_2-rich and SiC-depleted layers, and the thickness of the oxide layer depends on the SiC content. The addition of SiC improves the formation of the SiO_2 oxide layer, prevents further oxygen penetration, and thus, reduces the thickness of the oxide layer.

Keywords: ZrB_2-$MoSi_2$-SiC ceramics, SiC additive, thermophysical parameters, thermal shock resistance, oxide layers

I. Introduction

Zirconium diboride (ZrB_2) belongs to a group of ultra-high-temperature ceramic (UHTC) materials. High melting point (3 040 °C), high hardness (23 GPa), low density (5.8 g/cm^3), low resistance (16.6×10^{-5} Ω·cm), and high heat conductivity (24.27 W/m·K)[1–4] influenced a rapid development of this material for extreme high-temperature environments, e.g. for heat-shielding components in the aerospace industry, heating furnace components, and surface-protective materials. This remarkable material may be significant to overcome temperature, space, and speed limitations. However, oxidation of ZrB_2yields a highly evaporative B_2O_3 phase, which gradually decreases the oxidation resistance of ZrB_2. Moreover, inherent brittleness and poor thermal shock resistance limit to some extent its applications at high temperatures[5–7].

It was reported that the addition of $MoSi_2$ and SiC particles to ZrB_2 ceramic could improve the high-temperature performance[8–10]. These additives form a layer of SiO_2liquid glass phase, which suppresses O_2 permeation and enhances oxidation resistance. Furthermore, such additives significantly improve the physical and mechanical properties of ZrB_2 ceramics. The analysis of the cross-section of an oxidized ZrB_2-SiC sample indicated the existence of an oxidized transition layer, known as a SiC depletion layer[11, 12]. The SiC depletion layer improves the oxidation resistance and mechanical properties of the system and has a beneficial effect on thermal shock resistance. In the case of the ZrB_2-$MoSi_2$ system, $MoSi_2$can interact with ZrB_2 and O_2 to generate SiO_2, MoB, and ZrO_2 at high temperatures. Subsequently, SiO_2 and ZrO_2react and produce zirconium silicate $ZrSiO_4$, which is a prominent oxidation-resistant phase[2, 13]. Based on this, adding SiC and $MoSi_2$together to ZrB_2ceramics can also improve its oxidation resistance and mechanical properties. However, current research of the ZrB_2 composite system is mainly focused on mechanical properties and ablative resistance[14, 15]. Only a few studies have considered thermal shock resistance, especially with regard to application as a high-temperature surface coating. The key problem of the ZrB_2-$MoSi_2$-SiC system in the field of surface high-temperature oxidation resistance is inadequate thermal shock

* Corresponding author: ljyzq@163.com

resistance. Indeed, thermal shock resistance and associated physical properties (thermal conductivity, coefficient of thermal expansion, and elastic modulus,) require thorough investigation, along with the compositional design and preparation technology.

To determine the thermophysical properties and thermal shock resistance of ZrB_2-$MoSi_2$-SiC composite materials, we prepared 5 vol% and 15 vol% SiC-modified ZrB_2 – 15 vol% $MoSi_2$ceramics by means of spark plasma sintering (SPS). Thermal shock experiments were performed at different temperatures and times, and the effects of the SiC addition on thermal shock resistance, thermophysical properties, and microstructure were investigated.

II. Experimental

(1) Preparation of ZrB2-MoSi2-SiC composite materials

High-purity ZrB_2ceramic powders (purity ≥99.5 %, size 2.5 ± 0.5 μm), $MoSi_2$ (purity ≥99.9 %, size 1.5 ± 0.5 μm), and SiC (purity ≥99.9%, size 3 ± 0.5 μm) were mechanically mixed in the jar mill with ZrO_2 balls according to the volume ratio of ZrB_2-15 vol%$MoSi_2$-5 vol%SiC (ZMS5) and ZrB_2-15 vol%$MoSi_2$-15 vol%SiC (ZMS15). Milling was performed at a speed of 300 rpm for 6 h. The mixed powders were filtrated and dried in a vacuum oven. In the next step, dried powders were filled into a graphite mold and compacted to green bodies, and then sintered at 1 650 – 1 900 °C for 5 min with a heating rate of 150 K/min and external pressure of 40 MPa in the spark plasma sintering (SPS-20T-10) device. The cylindrical specimens with a diameter of 20 mm were obtained from the sintered bodies. The testing samples were cut into 2 mm × 3 mm × 7 mm blocks by means of wire-electrode cutting. After surface polishing, the samples were ultrasonically cleaned with anhydrous ethanol and then placed into an oven for further experimental testing.

(2) Performance testing and microstructural characterization

The water quenching method was used for the high-temperature thermal shock testing with the setting temperature of 1 000 and 1 200 °C. To clarify the relationship between material composition and thermal shock resistance and other thermophysical properties, we performed a single thermal shock test and then applied subsequent fivefold thermal shock tests. The single thermal shock test consisted of heating samples to the setting temperature and a dwell time of 5 min, followed by rapid immersion into cold water, which corresponds to sharp temperature changes. The subsequent thermal shock experiments consisted of reduced dwell time of 3 min at the peak temperature to prevent excessive oxidation. After water quenching, the samples were dried and the same experimental steps were repeated five times.

The density of sintered ceramics was measured with Archimede's method, and the determined value was compared with the theoretical density of the corresponding components to obtain the relative density of the material. The thermal expansion coefficient was tested on a device for determination of the thermal expansion coefficient (PCY-III) with the test temperature of 25 – 850 °C. The elastic modulus and strength were measured by means of nanoindentation (Nano Indenter G200). Thermal conductivity was determined with a laser thermal conductivity tester (NETZSCH LFA427).

The surface morphology investigation and elemental mapping were assessed by means of scanning electron microscopy with energy dispersive analysis (VEGA3-TESCAN). The phase composition of the samples was studied by means of X-ray diffractometry (BRUKER, D8 ADVANCE).

III. Results and Discussion

(1) Phase analysis and microstructural observations

The XRD patterns of the sintered ceramics are shown in Fig. 1. Both investigated ceramics exhibited the presence of ZrB_2, $MoSi_2$, and SiC phases. Furthermore, diffraction peaks of the ZrB_2 phase in ZMS15 shift slightly to the right and become sharpened compared to the ZMS5 ceramics, which originates from the higher SiC content. Diffraction peaks SiC in ZMS15 ceramics are more prominent than in ZMS5 ceramics, which indicates that a higher volume fraction of SiC particles is involved in the formation of the phase composition during the SPS processing.

Fig. 2 shows the microstructure of the sintered of ZMS5 and ZMS15 samples. Two different regions may be observed, gray and black ones, which probably originate from different phases. In addition to XRD, the EDS analysis revealed that the gray phase consists of Zr and B, which corresponds to ZrB_2, while, the black phase consists of Si and C, which corresponds to SiC phase. Moreover, a few features of the white phase (see the white arrow) can be found at the boundary region between ZrB_2 and SiC. According to the results of the EDS analysis, it consists of Mo and Si, which corresponds to $MoSi_2$. The obtained results are in agreement with those reported by Sciti[16], which showed that the $MoSi_2$additive promotes intercrystalline phase formation along the boundaries of ZrB_2 grains.

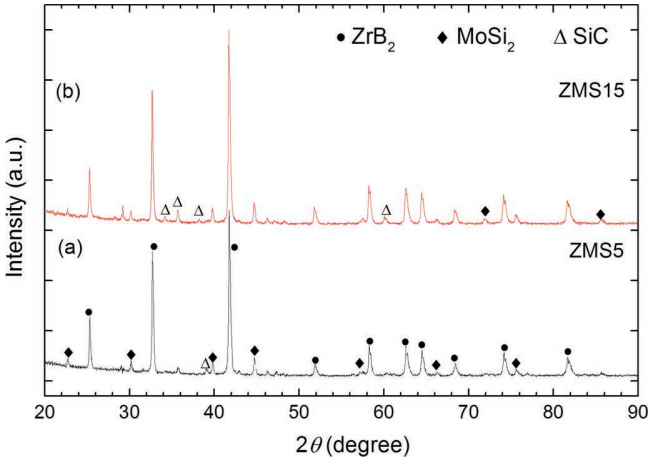

Fig. 1: XRD pattern of the sintered ceramics: (a) ZMS5, (b) ZMS15.

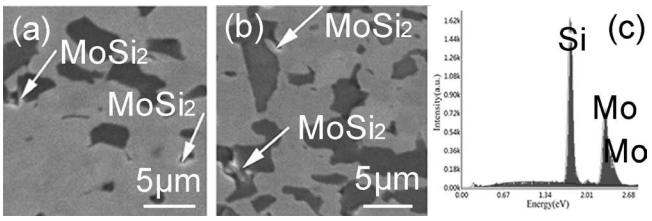

Fig. 2: SEM images of the surface morphology of the sintered ceramics and the EDS analysis of the white phase: (a) ZMS5, (b) ZMS15, (c) EDS analysis.

(2) Relative density

The density of samples was determined with Archimede's drainage method, and values of the calculated relative density are shown in Fig. 3. The relative density of the ceramics increases with the sintering temperature. The density of ZMS15 ceramics is 5.18 g/cm^3 with the nearly fully dense material at the sintering temperature of 1 900 °C. Also, the relative density of ZMS15 is higher than that of ZMS5, independent of the sintering temperature. It indicates that the increase of the SiC additive amount is beneficial and promotes the densification of the sintered body. It is well established that, owing to its strong covalent bonding and a low self-diffusion coefficient, ZrB_2 has a poor sintering performance and requires high sintering temperatures to achieve high density. The addition of SiC additive inhibits grain boundary migration rate during sintering and recrystallization of ZrB_2 grains[17–20]. This improves material performance and reduces sintering temperature. Meanwhile, the $MoSi_2$additive phase also plays a role as a sintering aid and enhances the density due to its low dihedral angle and good wettability[21,22]. The more SiC, the better the sintering performance. Therefore, ZMS15 ceramics can be sintered to nearly fully dense material at lower sintering temperatures.

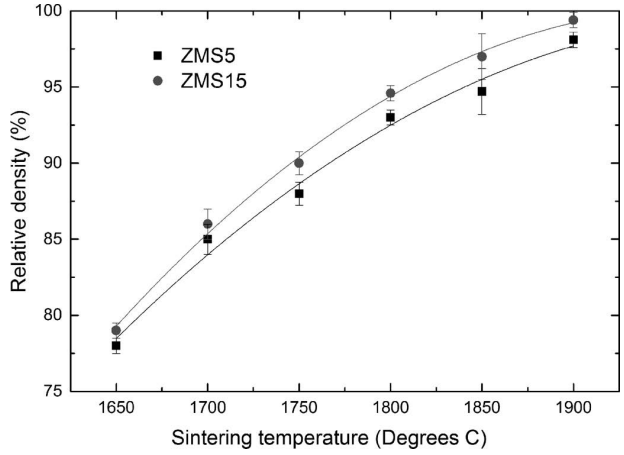

Fig. 3: The relative density of the testing ceramics at different sintering temperatures.

(3) Thermophysical parameters

The thermophysical properties of high-temperature ceramics are closely related to their thermal shock resistance. Owing to high thermal conductivity, the internal temperature increase and short-term thermal stresses are quickly dispersed and alleviated, which is beneficial for the thermal resistance of the material[23,24]. A low thermal expansion coefficient of the ceramics has the same effect. Therefore, the focus of the investigation is on the fabrication of ceramics with high thermal conductivity and a low thermal expansion coefficient. We measured the thermal conductivity and specific heat capacity and the results are shown in Table 1 and Fig. 4, respectively. Both the thermal conductivity and the specific heat capacity of ZMS15 are higher than that of ZMS5. It indicates the beneficial effect of SiC for heat transfer. The change in the thermal expansion coefficient (CET) with temperature is sharp before 400 °C and then slows down between 400 ~ 850 °C. ZMS15 ceramics exhibit a lower CET than ZMS5 ceramics. Even at the peak temperature, the CET of ZMS15 remains below 9.2 × 10^{-6}/K and of ZMS5 above 10 × 10^{-6}/K. It confirms again that the addition of the SiC phase is a feasible method to reduce the CET and the thermal stress concentration.

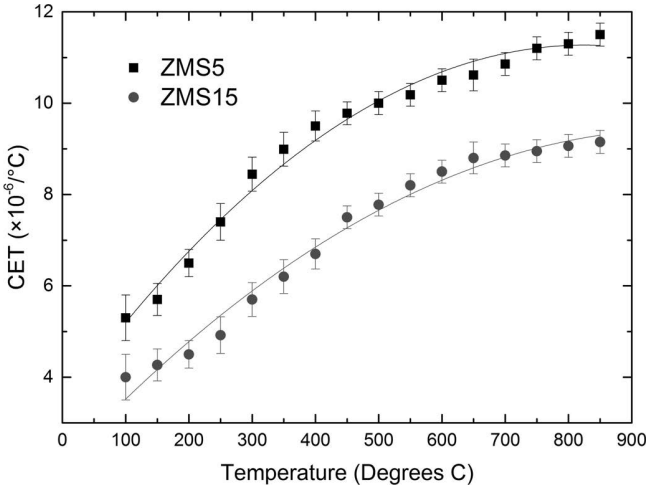

Fig. 4: Influence of different SiC contents on thermal expansion coefficient of samples.

Table 1: Thermal conductivity and specific heat capacity of the two components at 1 200 °C

Ceramics	Thermal conductivity (W/m/K)	Specific heat capacity (J/kg/K)
ZMS5	49	388
ZMS15	57	451

Undoubtedly, a few cracks might emerge in the sample exposed to temperature changes. Therefore, the properties of the ceramics should be improved to prevent crack propagation. Hasselman[25] proposed the R_{st}(thermal stress crack stability factor) definition, as shown in equation (1):

$$R_{st} = \left(\frac{\lambda^2 G}{\alpha_t^2 E_0}\right)^{\frac{1}{2}} \quad (1)$$

where E_0 is the elastic modulus of the material, λ is the thermal conductivity, G is a crack propagation force, and α is a thermal diffusion coefficient. The thermal stress crack stability factor determines whether the crack tends to extend further. It indicates that the thermal stress crack stability factor is inversely proportional to the elastic modulus.

Table 2: Elastic modulus test results of two components

Ceramics	Elastic modulus (GPa)
ZMS5	542.1
ZMS15	489.7

Fig. 5 shows the modulus-depth curves of ZMS ceramics. The elastic modulus curve is unstable if the penetration depth is within 100 μm, which is caused by surface roughness and surface hardening of the sample during grinding and polishing. At the penetration depth above 400 μm, the curves gradually stabilize. So, we choose values from 400 to 900 μm to obtain the measurement data. Each sample was tested at five points and the average value was calculated. It can be found that the elastic modulus of the ceramics decreases with the addition of SiC. It also suggests that SiC has a beneficial influence on preventing the crack r extension.

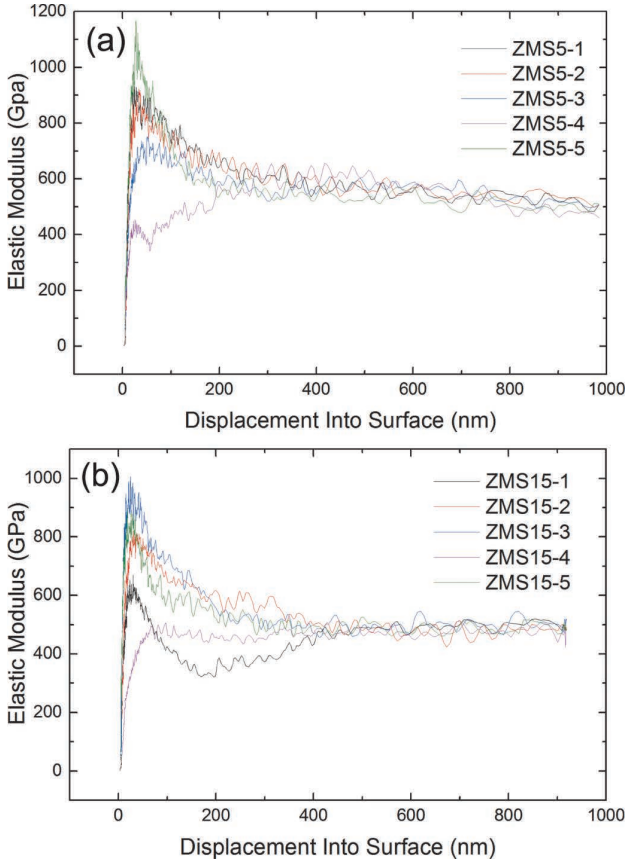

Fig. 5: Modulus-depth curves of ZMS5 (a) and ZMS15 (b).

(4) Single thermal shock test

XRD patterns of the oxide phase after the single thermal shock experiment at different temperatures for both ceramics are shown in Fig. 6. The main oxidation phases are ZrO_2, SiO_2, and $ZrSiO_4$. Moreover, the diffraction peak intensity of oxide phases of ZMS15 is stronger than that of ZMS5, and that results are the same at all investigated temperatures. This reveals that the higher SiC content and a higher temperature promote the oxidation reaction. Therefore, more oxidation products are generated, and more complete SiO_2 oxide layers are formed subsequently, which yields a lower diffraction peak intensity of the matrix phase. Especially, the peak intensity of the matrix phase in ZMS15, Fig. 7d, is lower in comparison to the peak intensity of the SiO_2, ZrO_2, and $ZrSiO_4$ phases.

Fig. 7 shows surface morphology and the EDS analysis results for both ZMS ceramics after thermal shock experiments at 1 000 and 1 200 °C. The observed microstructure shows that a protective layer composed of black bulk phase and dispersed white nodule

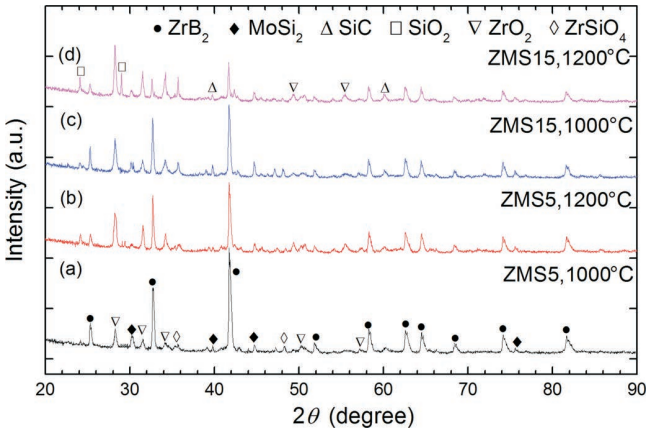

Fig. 6: XRD patterns of the specimen surface after single thermal shocks test: (a) and (b) ZMS5 at 1 000 °C and 1 200 °C, respectively; (c) and (d) ZMS15 at 1 000 °C and 1 200 °C, respectively.

particles is formed on the surface of ceramics. Combined EDS and XRD results indicate that the black bulk phase is SiO_2 and the small white nodule particles are ZrO_2 and $ZrSiO_4$. Furthermore, the sintering temperature and SiC content impact the morphology and distribution of the protective layer, especially of the SiO_2 phase. The oxidized surface of ZMS5 is dominantly covered by small nodules with a scattered SiO_2 phase, whereas the surface of ZMS15 ceramic is covered with a continuous SiO_2 protective layer. As a comparison, the influence of the experimental temperature is more significant. After the thermal shock experiment at 1 200 °C, the entire surface is covered by a protective layer. Besides, no microcracks can be observed on the oxidized surface. It indicates that the continuous glassy structure of SiO_2 phase with the wrapped nodules has a good thermal shock resistance to avoid the initial crack formation.

Generally, during the thermal shock experiment, the ZrB_2-$MoSi_2$-SiC system inevitably undergoes a high-temperature oxidation reaction. The oxidation behavior of each component is as follows[13, 26]:

$$ZrB_2(s) + 2.5 = O_2(g) = ZrO_2(s) + B_2O_3(g) \quad (2)$$

$$SiC(s) + 1.5O_2(g) = SiO_2(s) + CO(g) \quad (3)$$

$$MoSi_2(s) + 3.5O_2(g) = MoO_3(g) + 2SiO_2(g) \quad (4)$$

Meanwhile, $MoSi_2$ can react with ZrB_2 in oxygen, the reaction equation of which is as follows[26]

$$ZrB_2(s) + 2MoSi_2(s) + 5O_2(g) = ZrO_2(s) + 2MoB(s) + 4SiO_2(s) \quad (5)$$

According to the previously published research[26], the sequential order of oxidation in this system is (2)→(3)→(4)/(5). Therefore, ZrB_2 firstly undergoes an

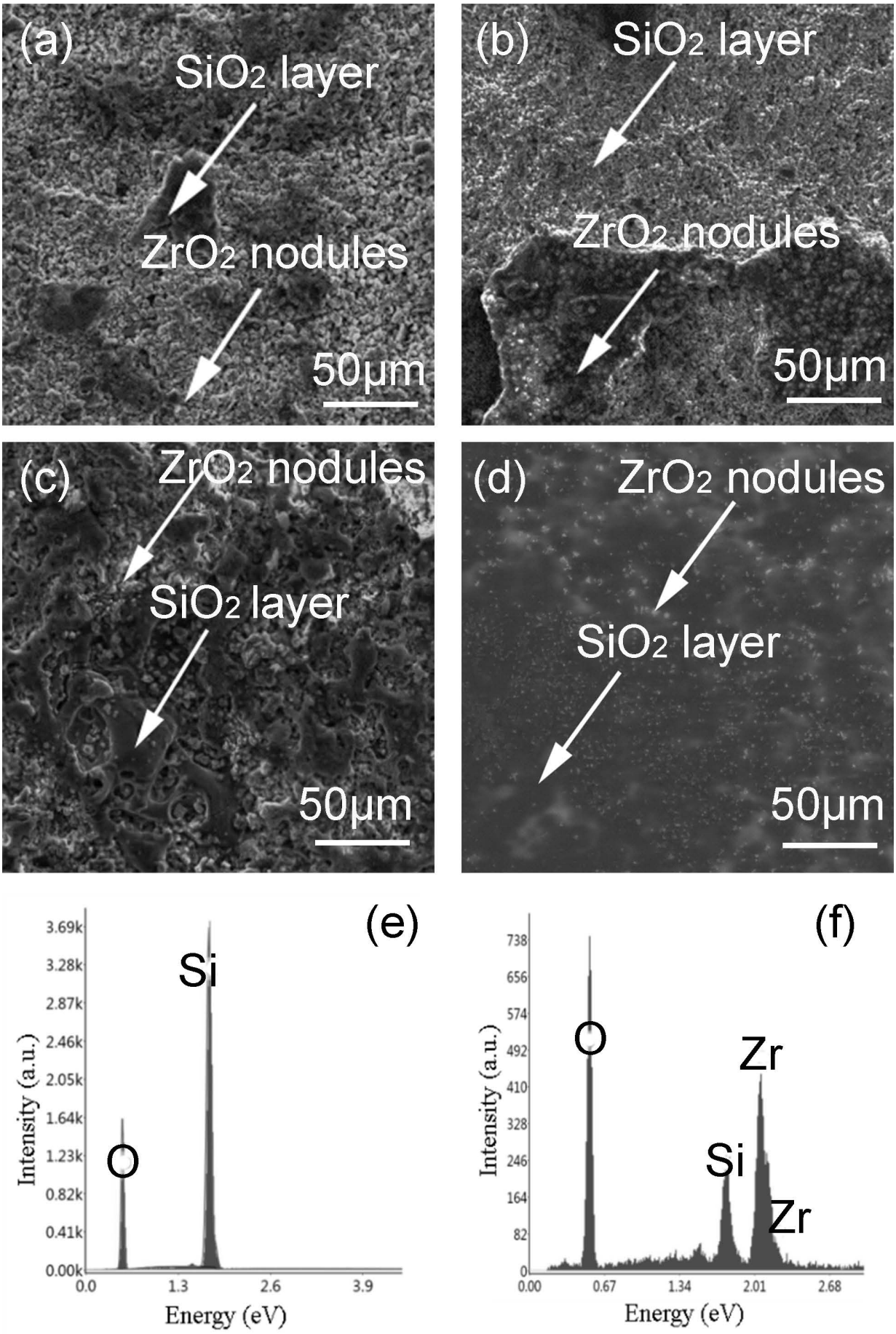

Fig. 7: SEM images of the oxide surface after single thermal shocks test: (a) and (b) ZMS5, at 1 000 °C and 1 200 °C, respectively; (c) and (d) ZMS15, at 1 000 °C and 1 200 °C, respectively; (e) and (f) EDS spectra of oxidation layer and nodules particles.

oxidation reaction to generate small nodules of ZrO_2 and B_2O_3, and then SiC and $MoSi_2$ subsequently oxidize to generate SiO_2. Owing to a low melting point, SiO_2 readily forms a glass layer to wrap the ZrO_2nodules with their higher melting point, and then the silicate $ZrSiO_4$ phase is generated. Because the SiO_2 phase in the system is mainly obtained through the oxidation of SiC, the coverage of SiO_2 layer on the sample surface increases as a higher amount of additive SiC is added into the ZMS ceramics. Moreover, the increase of temperature accelerates the oxidation of SiC and improves the fluidity of the SiO_2 phase. Therefore, the entire ceramic matrix can be covered and protected by a complete oxidation-resistant layer.

(5) Fivefold thermal shock experiment

Fig. 8 shows the oxidized surface morphology after the fivefold thermal shock test at the temperature of 1 000 °C. It can be seen that the entire oxide surface is composed of the black SiO_2 phase and the white composite oxide phase, ZrO_2 and $ZrSiO_4$. The main difference between these shock tests is the volume fraction of phases. The volume fraction of the SiO_2 phase and the composite oxide phase progressively increased with the number of thermal shock tests. Owing to the excellent fluidity of the SiO_2 phase, the oxide surface morphology gradually transforms from discontinuous oxide particles in the layer to a uniform glassy oxide layer, and the composite oxide phase distributes diffusively in the glassy oxide layer. Meanwhile, the area covered also increases with the number of thermal shock tests. In this present study, after the third or fourth thermal shock experiments, the sample surface is completely covered by the oxidation-protective layer.

Besides the number of thermal shock tests, the influence of the SiC content on the thermal shock resistance is also discussed. Since ZMS5 possesses a lower volume fraction of SiC, the protective layer was not completely formed until the fourth thermal shock experiment, whereas for ZMS15 it was achieved after the third thermal shock experiment. It confirms that SiC is beneficial for the rate of SiO_2 formation and thermal shock resistance of the ZMS ceramics.

The unfavorable formation of pores on the surface of the investigated sample after the first thermal shock test was more apparent in ZMS15. However, the subsequent thermal shock experiment causes the pores to disappear. According to the oxidation equation (3), when O_2 permeates into the ceramics and reacts with SiC, gaseous CO gas could be generated. In the first thermal shock test, CO gas is partially entrapped by the solidified oxide layer, and then the gas pores form, Figs. 8a and 8 f. In the subsequent thermal shock test, previously solidified oxide layers are reheated, which favors the release of entrapped CO gas. Meanwhile, the excellent fluidity of the SiO_2 phase formed in the subsequent thermal shock experiment contributes to the filling and elimination of the pores. The formed oxidation-resistant layer can prevent oxygen erosion from continually generating CO gas. Thus, the pores are gradually eliminated and cannot be observed in the subsequent SEM micrographs.

(6) Crack initiation and propagation of thermal shock resistance

In the present study, after the thermal shock experiment, crack and fracture formation commonly occur in the high-temperature ceramic. Therefore, the reduction of the crack initiation and propagation, and improvement of the thermal shock resistance for ZrB_2 ceramics is still a challenge. Fig. 9 shows the SEM micrographs of the crack morphology after the first thermal shock test at the temperature of 1 000 °C. It was found that some microcracks appear in the SiO_2 phase which propagation stops at the boundary of SiO_2, Fig. 9a. This is probably caused by the shrinkage stress. After rapid water quenching, the isolated bulk glassy oxide SiO_2 phase solidified and formed. The instantaneous shrinkage stress derived from the volume shrinkage and thermal contraction is large enough to generate the initial microcracks in the glassy SiO_2 phase. Also, Fig. 9(b), other microcracks originate from the small composite oxide nodules. These initial microcracks are due to the volume expansion of ZrO_2, and the difference of the thermal expansion coefficient between the ZrO_2 and SiO_2. Besides, the crack deflection can be observed when the crack encountered and passed through the ZrO_2 nodules, Fig. 9c. However, in the subsequent thermal shock experiments, those initial microcracks gradually disappeared, and the oxide layer became smooth and complete, especially for the ZMS15 ceramics, Fig. 9d. This is because the reheated SiO_2 phase has an excellent self-repairing ability to fill in the microcracks. On the other hand, the SiC additive promotes thermal conductivity, decreases the thermal expansion coefficient and elastic modulus, which is beneficial to reduce the shrinkage stress, providing excellent thermal stability.

During the thermal shock resistance experiments, the O_2 erosion mainly affects surface microstructure and performance of ceramics. The severity of O_2 erosion mainly depends on the oxidation resistance of the ceramics itself. Beyond that, a certain number of defects (cracks, gas pores, etc.) are generated during the temperature and can facilitate oxygen infiltration into the sample. To clarify the mechanism of the oxidation resistance and thermal shock resistance, we assessed the thickness of the oxide layer and the chemical composition. Fig. 10 shows the SEM and EDS analysis of the cross-section after the fifth thermal shock experiment at 1 200 °C. The EDS analysis was performed on the red area marked on the SEM micrograph of the cross-section.

According to the elemental distribution determined by the EDS analysis, the cross-section layer can be divided into three regions from the surface to the center: the outermost oxide layer, Fig. 10, I layer, the intermediate transition layer Fig. 10, II layer, and the inner ceramic body, Fig. 10, III layer. The formation of these three regions is following the outward diffusion process of the oxidizable elements in the ceramic body and the inward diffusion of oxygen. The outermost oxide layer is a SiO_2-rich layer formed by the Si out-diffusion and reaction with oxygen at high temperatures. Owing to a low melting point and high fluidity, the SiO_2 layer covered the surface of the ceramic body in the outmost layer.

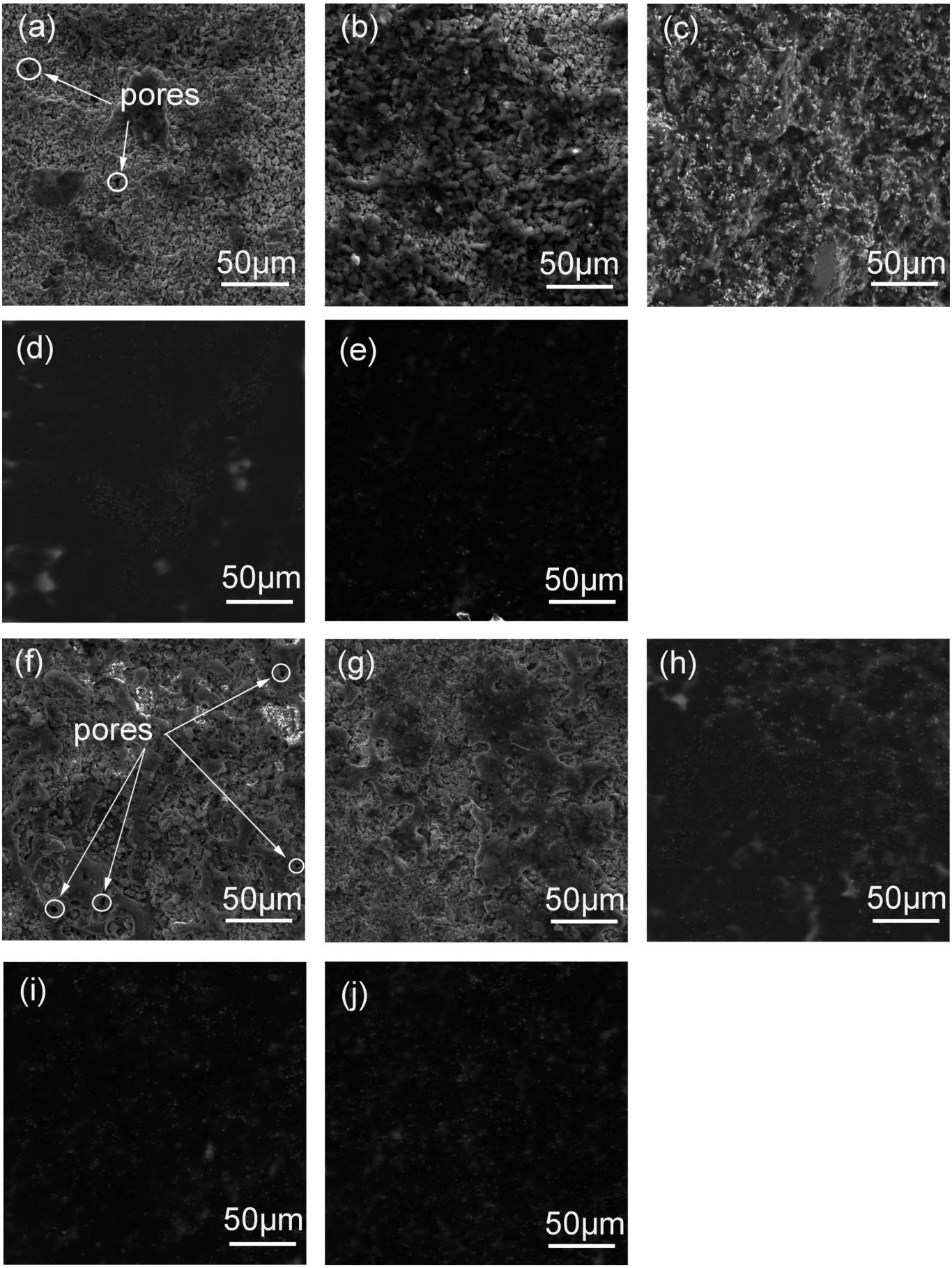

Fig. 8: SEM images of the oxide surface morphologies after five times thermal shocks test. (a) -(e) for each ZMS5; (f) -(j) for each ZMS15.

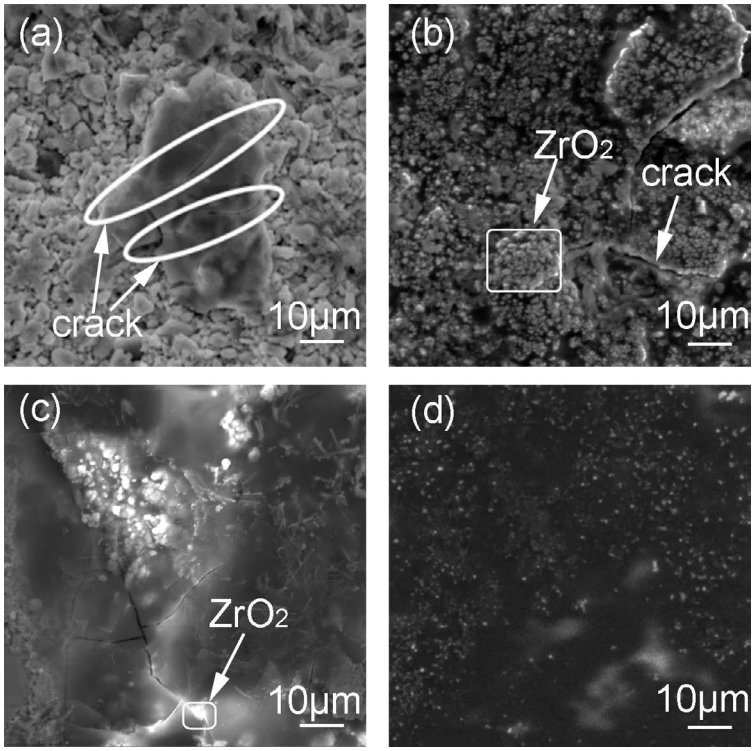

Fig. 9: SEM images of the crack morphologies after thermal shocks test at the temperature of 1 000 °C. (a) and (b) ZMS5 and ZMS15 after single thermal shock test, respectively; (c) crack deflection in ZMS15; (d) ZMS15 five-times thermal shock test.

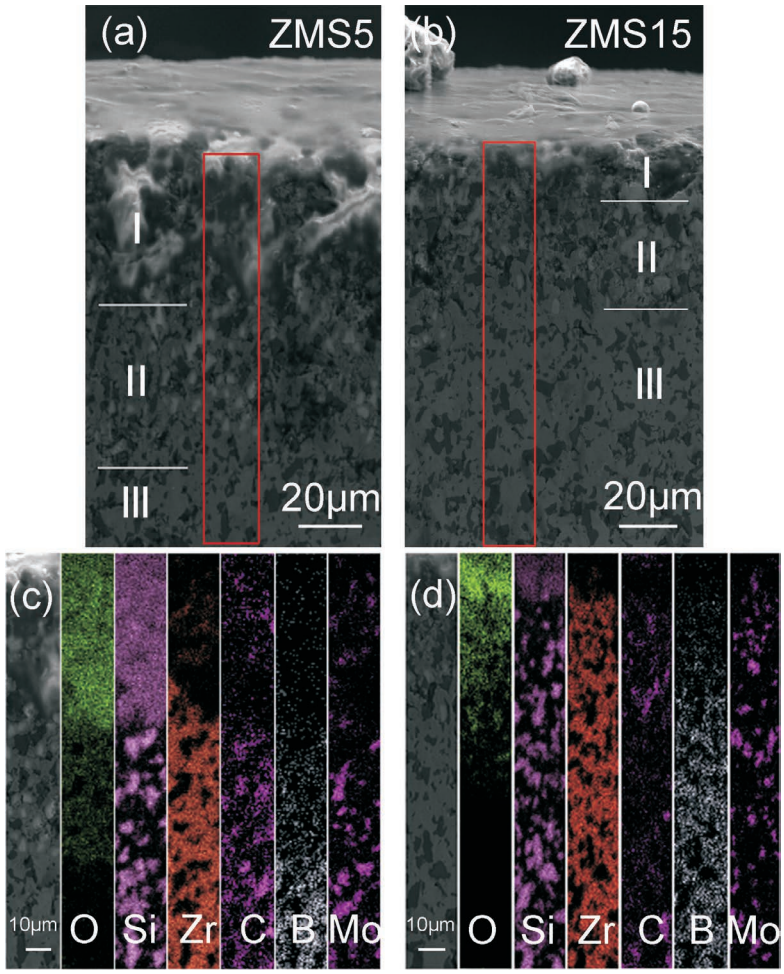

Fig. 10: The cross-sections, SEM images and EDS analysis of the ceramics after fifth thermal shock experiment at 1 200 °C: (a) ZMS5 ceramics, (b) ZMS15 ceramics, (c) EDS mapping for ZMS5, and (d) EDS mapping for ZMS15.

The intermediate transition layer is a SiC consumption layer and the main oxide phase is ZrO_2. The high affinity between SiC and O_2 yields a faster oxidation rate than in the case of ZrB_2 and $MoSi_2$. It can be seen from Fig. 10(c) and (d) that Si content in the oxide layer gradually decreases with the oxidation depth, and a significant amount of ZrO_2 appears. However, SiC in the transition layer cannot be completely depleted because of the increased thickness of the protective layer and the decreasing content of the in-diffused oxygen during the continual thermal shock resistance experiments. At the bottom is the unreacted area while the original microstructure is maintained.

In a comparison between the ZMS5 and ZMS15 oxide layers, it can be seen that the thickness of the oxide layers is considerably different because there is a different SiC volume fraction. The thickness of the oxide layer of ZMS5 reached 40 μm, while it is only 15 μm for ZMS15 ceramics. However, the thickness of the transition layer is similar, being 30 and 25 μm for ZMS5 and ZMS15 ceramics, respectively. These results confirm that the SiC additive plays an important role in the SiO_2oxidation process. The SiO_2 phase covers the ceramics surface and prevents deep penetration of O_2 into the main ceramic body. An increasing volume fraction of SiC enhances the protective area of the SiO_2 layer in the high-temperature oxidizing environment, promotes the isolation of O_2, and decreases the O_2 reaction zone. Although the increase of SiC has little effect on the thickness of the SiC consumption layer, the ratio between the SiC consumption layer and the outermost SiO_2 layer increased from 3/4 to 5/3 in the ZMS15 ceramics. This decreases the internal stress generated by the volume expansion of the material. Therefore, ZMS15 ceramics exhibited excellent thermal shock resistance.

IV. Conclusions

High-performance ZrB_2-$MoSi_2$-SiC (ZMS) ceramics with excellent thermal shock resistance were successfully fabricated by optimization of the SiC amount in the material and spark plasma sintering.

1. A higher volume fraction of SiC additive enhances thermophysical parameters in a way that thermal conductivity increases, while the thermal expansion coefficient and elastic modulus decrease, which is beneficial for improving thermal shock resistance.

2. High SiC content and high temperatures accelerate the oxidation of SiC and the formation of an oxidation-resistant layer. The smooth oxidized layer is composed of a continuous glassy structure of the SiO_2 phase with wrapped ZrO_2 and $ZrSiO_4$ nodule phases, which can fully cover the whole ZMS15 ceramics surface and contribute to thermal shock resistance.

3. Entrapped gas pores can be generated on the oxidized surface because of the CO gas released during the first thermal shock test. These pores are filled with the flowing SiO_2 phase and eliminated during the subsequent test.

4. Owing to large shrinkage stress derived from a discontinuous and insufficient amount of the SiO_2 phase in the first thermal shock test, the volume expansion of ZrO_2, and the mismatch of the thermal expansion coefficient between the oxide phases, microcracks can be observed on the surface after the first thermal shock. However, these microcracks can be self-repaired by the sufficient and melt-flowing SiO_2 phase in the subsequent thermal shock tests.

5. The oxide layer can be divided into the SiO_2-rich layer and the SiC-depleted layer. High SiC content can increase the ratio between the SiC consumption layer and the outermost SiO_2 layer, and then decrease the internal stress and improve the thermal shock resistance.

Acknowledgements

This work is supported by the National Natural Science Foundation of China (No. 51901069), Program for Changjiang Scholars and Innovative Research Team in University of Ministry of Education of China (Grant No. IRT_1234) and the Non-ferrous Metal Generic Technology Collaborative Innovation Center of Henan Province.

References

1 Jayaseelan, D.D., Wang, Y., Hilmas, G.E., Fahrenholtz, W., Brown, P., Lee, W.E.: TEM investigation of hot pressed-10 vol% SiC-ZrB_2 composite, *Adv. Appl. Ceram.*, **110**, [1], 1–7, (2011).

2 Guo, S.Q.: Densification of ZrB_2-based composites and their mechanical and physical properties: a review, *J. Eur. Ceram. Soc.*, ***29**, [6], 995–1011, (2009).*

3 Sun, Y., Xiao, X., Chai, G., Xu, G., Xiong, B., Zhang, S.: Microstructure, optical properties and thermal stability of ZrB_2 and Zr-B-N thin films as high-temperature solar selective absorbers, *Mater. Express, **4**, [3], 205–212, (2014).*

4 Chamberlain, A.L., Fahrenholtz, W.G., Hilmas, G.E.: Pressureless sintering of zirconium diboride, *J. Am. Ceram. Soc., **89**, [2], 450–456, (2006).*

5 Akgun, B., Çamurlu, H.E., Topkaya, Y., Sevinç, N.: Mechanochemical and volume combustion synthesis of ZrB_2, *Int.J.Refract.Met.Hard Mater.*, **29**, [5], 601–607, (2011).

6 Zhang, Y., Hu, Z., Yang, B., Ren, J., Li, H.: Effect of pre-oxidation on the ablation resistance of ZrB_2-SiC coating for SiC-coated carbon/carbon composites, *Ceram. Int., **41**, [2], 2582–2589, (2015).*

7 Wang, L., Liang, J., Wan, X.: Mechanical properties and thermal shock resistance of anisotropic ZrB_2-SiC-graphite ceramic, *Ceram. T., **248**, 529–534, (2014).*

8 Silvestroni, L., Meriggi, G., Sciti, D.: Oxidation behavior of ZrB_2 composites doped with various transition metal silicides, *Corros. Sci., **83**, 281–291, (2014).*

9 Silvestroni, L., Landi, E., Bejtka, K., Chiodoni, A., Sciti, D.: Oxidation behavior and kinetics of ZrB_2 containing SiC chopped fibers, *J. Eur. Ceram. Soc., **35**, [16], 4377–4387, (2015).*

10 Sarin, P., Driemeyer, P.E., Haggerty, R.P., Kim, D.K., Bell, J.L., Apostolov, Z.D., Kriven, W.M.: In situ studies of oxidation of ZrB_2 and ZrB_2-SiC composites at high temperatures, *J. Eur. Ceram. Soc., **30**, [11], 2375–2386, (2010).*

11 Pourasad, J., Ehsani, N., Valefi, Z.: Oxidation resistance of a SiC-ZrB_2 coating prepared by a novel pack cementation on SiC-coated graphite, *J. Mater. Sci., **52**, [3], 1639–1646, (2017).*

12 Zhang, X., Xu, L., Du, S., Han, J., Hu, P., Han, W.: Fabrication and mechanical properties of ZrB_2-SiCw ceramic matrix composite, *Mater. Lett.*, **62**, [6–7], 1058–1060, (2008).

13 Guo, S.Q., Mizuguchi, T., Aoyagi, T., Kimura, T., Kagawa, Y.: Quantitative electron microprobe characterizations of oxidized ZrB_2 containing $MoSi_2$ additives, *Oxid. Met., **72**, [5–6], 335, (2009).*

14 Iatsyuk, I.V., Potanin, A.Y., Rupasov, S.I., Levashov, E.A.: Kinetics and high-temperature oxidation mechanism of ceram-

ic materials in the ZrB_2-SiC-$MoSi_2$ system, *Russ. J. Non-Ferr. Met.,* ***59****, [1], 76–81, (2018).*

15 Paul, T.R., Mondal, M.K., Mallik, M.: Microstructure dependent physical and mechanical properties of spark plasma sintered ZrB_2-$MoSi_2$-SiCw composites, *Int. J. Refract. Met. Hard Mater.,* **79**, 131–137, (2019).

16 Sciti, D., Guicciardi, S., Bellosi, A., Pezzotti, G.: Properties of a pressureless-sintered ZrB_2-$MoSi_2$ ceramic composite, *J. Am. Ceram. Soc.,* ***89****, [7], 2320–2322, (2006).*

17 Wang, W., Sun, K., Liu, H.: Effects of different aluminum sources on morphologies and properties of ceramic floor tiles from red mud, *Const. Build. Mater.,* **241**, 118119. (2020).

18 Zhang, L., Wei, C., Li, S., Wen, G., Liu, Y., Wang, P.: Mechanical and thermal shock properties of laminated ZrB_2-SiC/SiCw ceramics, *Ceram. Int.,* ***45****, [5], 6503–6508, (2019).*

19 Li, W., Zhang, X., Hong, C., Han, W., Han, J.: Microstructure and mechanical properties of zirconia-toughened ZrB_2-$MoSi_2$ composites prepared by hot-pressing, *Scr. Mater.*, **60**, [2], 100–103, (2009).

20 Fahrenholtz, W.G., Hilmas, G.E., Talmy, I.G., Zaykoski, J.A.: Refractory diborides of zirconium and hafnium, *J. Am. Ceram. Soc.,* ***90****, [5], 1347–1364, (2007).*

21 Monteverde, F.: The addition of SiC particles into a $MoSi_2$-doped ZrB_2 matrix: effects on densification, microstructure and thermo-physical properties, *Mater. Chem. Phys.,* ***113****, [2–3], 626–633, (2009).*

22 Silvestroni, L., Sciti, D., Kling, J., Lauterbach, S., Kleebe, H.J.: Sintering mechanisms of zirconium and hafnium carbides doped with $MoSi_2$, *J. Am. Ceram. Soc.,* ***92****, [7], 1574–1579, (2009).*

23 Mallik, M., Kailath, A.J., Ray, K.K., Mitra, R.: Electrical and thermophysical properties of ZrB_2 and HfB_2 based composites, *J. Eur. Ceram. Soc.,* ***32****, [10], 2545–2555, (2012).*

24 Zimmermann, J.W., Hilmas, G.E., Fahrenholtz, W.G., Dinwiddie, R.B., Porter, W.D., Wang, H.: Thermophysical properties of ZrB_2 and ZrB_2-SiC ceramics, *J. Am. Ceram. Soc.,* ***91****, [5], 1405–1411, (2008).*

25 Hasselman, D.P.H., Donaldson, K.Y., Anderson, E.M., Johnson, T.A.: Effect of thermal history on the thermal diffusivity and thermal expansion of an alumina-aluminum titanate composite, *J. Am. Ceram. Soc.,* ***76****, [9], 2180–2184, (2005).*

26 Guo, S., Mizuguchi, T., Ikegami, M., Kagawa, Y.: Oxidation behavior of ZrB_2-$MoSi_2$-SiC composites in air at 1500 °C, *Ceram. Int.,* ***37****, [2], 585–591, (2011).*